Synthesis, characterization, and functionalization of ZnO nanoparticles by N-(trimethoxysilylpropyl) ethylenediamine triacetic acid (TMSEDTA): Investigation of the interactions between Phloroglucinol and ZnO@TMSEDTA

Haythem Barrak[1], Taieb Saied[2], Pascale Chevallier[3,4], Gaétan Laroche[3,4], Adel M'nif[1], and Ahmed Hichem Hamzaoui[1]

[1]Laboratoire de Valorisation des Matériaux Utiles, Centre National de Recherche en Sciences des Matériaux, Technopole BorjCédria, BP, route touristique de Soliman, Tunisia
[2]Département de Chimie et de Biologie Appliquées, Institut National des Sciences Appliquées et de Technologie, BP 676, 1080 Tunis Cedex, Tunisia
[3]Laboratoire d'Ingénierie de Surface (LIS), Département de Génie des Mines, de la Métallurgie et des Matériaux, Centre de Recherche sur les Matériaux Avancés (CERMA), Université Laval, 1065 avenue de la médecine, Québec G1V 0A6, Canada
[4]Centre de Recherche du CHU de Québec, Axe Médecine Régénératrice, Hôpital St-François d'Assise, 10 rue de l'Espinay, Québec G1L 3L5, Canada

ABSTRACT
The use of semiconductor oxides, such as chemical or biological sensors, requires their functionalization with appropriate molecules displaying specific interaction with the substance to be detected. Generally, the support materials used are TiO_2 or SiO_2. In the present work, zinc oxide nanoparticles (ZnO NPs), known for its reactivity and high specific area, were used. The synthesis of nanoscale ZnO was advantageously performed by precipitation at low temperature (60 °C). To our knowledge, it was the first time that this material was synthesized at such a low temperature, therefore lowering production cost. Moreover, the surface functionalization of ZnO was performed with N-(trimethoxysilylpropyl) ethylenediamine triacetic acid (TMSEDTA) in ethanol. This allowed shortening the functionalization reaction duration as compared to previously published literaturein the field. The samples obtained were analyzed by XRD, TEM, DLS, FTIR, TGA and XPS, which all concur with the successful synthesis of ZnO nanoparticles as well as the efficiency of TMSEDTA grafting on ZnO. Then, the interactions of this functionalized material, ZnO@TMSEDTA, with the Phloroglucinol (drug) were evaluated by using cyclic voltammetry measurements in solution. The cyclic voltammograms showed an intense cathodic peak which was correlated to the initial concentration of free Phloroglucinol. This cathodic peak was degraded upon addition of ZnO@TMSEDTA particles due to the drug interactions with free available carboxylic groups on the functionalized NPs. Based on a calibration curve, the drug concentration uptake can be therefore quantified. Thus, these results establish a big step to develop a Phloroglucinol sensor.

KEYWORDS
ZnO, nanoparticle, functionalization, Drug interactions, phloroglucinol

CITATION
Barrak, H., Saied, T., Chevallier, P., Laroche, G., M'nif, A., & Hamzaoui, A. H. (2016). Synthesis, characterization, and functionalization of ZnO nanoparticles by N-(trimethoxysilylpropyl) ethylenediamine triacetic acid (TMSEDTA): Investigation of the interactions between Phloroglucinol and ZnO@ TMSEDTA. Arabian Journal of Chemistry.

1 INTRODUCTION

The preservation of drinking water quality through the monitoring organic pollutants is a current concern worldwide. For this purpose, technical analysis resources are available to quantitatively measure the level of various pollutants. NMR spectroscopy, liquid chromatography, atomic absorption spectrophotometry and mass spectrometry count among these techniques (Zaideh et al., 2001). However, these latter analytical techniques are rather time consuming and require quite expensive hardware and infrastructure. To minimize the cost of analyses, scientists are therefore focusing their efforts on developing materials and nanomaterials-based sensors and biosensors (Li et al., 2012; Chan and Fale, 2014). For instance, several research groups have already developed functionalized surfaces by several biological molecules and chemical molecules (Wang et al., 2015; Yu et al., 2009) to increase the sensitivity of these sensors (Gupta et al., 2012). Recent researches have focused on the detection of gases (Irajizad and Mortezaali, 2015), enzymes (Wang et al., 2008; Cao et al., 2011; Dönmez et al., 2014), pesticides (Guan et al., 2012) and other organic pollutants (Dennison and Turner, 1995) with hybrid materials in which inorganic compounds were functionalized with organic molecules (Wang et al., 2012). For example, gold (Shukla et al., 2012), platinum, metal oxides such as TiO2 (Li et al., 2013), Fe_3O_4 (Qian et al., 2014) and ZrO_2 (Su et al., 2011) were already considered, thanks to their semiconducting properties. On the organic molecule side, silanes such as 3-(aminopropyl) trimethoxysilane APTMS, (Mora et al., 2007; Tan et al., 2011) 3-(aminomethyl) trimethoxysilane AMTMS and N-[3-(trimethoxysilyl)propy] ethylenediamine triacetic acid trisodium salt) (De Palma et al., 2007), were currently used, but also phosphates and carboxylic acids were also investigated (Desmet et al., 2012). The conjugations of these organic molecules are done in order to functionalize the NPs with specific chemical groups allowing the detection of the targeted molecules, such as pollutants, and drugs.

Indeed, drugs are new forms of water pollution (Xie et al., 2010), which threaten the environment. Indeed, in several studies, scientists proved the presence of traces of pharmaceuticals in water such as sleeping pills, antidepressants, aspirin, contraceptive and anti-inflammatory (Dévier et al., 2013; Duan et al., 2013). These drug traces are mainly coming from drugs discharged into the aquatic environment in particular in wastewater of hospitals and pharmaceutical industry (Bailly et al., 2013; Marcu and Viespe, 2015; Acuautla et al., 2014). Currently, the ZnO nanoparticles (Huang et al., 2008) have been explored for detecting toxic gases (Choi and Kim, 2012) and as biological sensors (Deng et al., 2008). At this step, regarding the application, it is of paramount importance to develop functionalized nanoparticles in the ‘‘more ecofriendly environment”, meaning easily handle, with no harsh organic solvents and molecules. In order to minimize the impact on the environment, an original synthesis of ZnO particles has been developed in aqueous solution without surfactants at low temperature (60 °C) in ammonia aqueous solution from zinc acetate salt. Thereafter, the functionalization of ZnO particles has been performed in ethanoic solution with N-(trimethoxysilylpropyl) ethylenediamine triacetic acid (TMSEDTA). The choice of TMSEDTA was not trivial because this molecule should respond to severe criteria. Indeed, the molecule should strongly interact with the ZnO particles, should permit to reach a good dispersion of the particles in the medium used for the drug detection, but also should lead to free receptors that will further establish low energy bonds with the antibiotic. This last parameter is chosen because it thus becomes possible to separate thereafter the antibiotic from the initial ZnO particles. In this case, based on a reusable electrode of ZnO@TMSEDTA, an electrochemical cell can be envisaged for fast antibiotic detection and quantification.

In this context, the objective of this work was to present a solid proof of concept demonstrating the possibility of developing a drug sensor, by conjugating N-(trimethoxysilylpropyl) ethylenediamine

triacetic acid (TMSEDTA) on zinc oxide ZnO nanoparticles in surfactant-free aqueous solution at relatively low temperature (60 °C). The effects of ZnO NPs coated with TMSEDTA on the oxidation intensity current of the drug (Phloroglucinol) in water solution were clearly evidenced by voltammetry. Furthermore, the decrease in the peak intensity of Phloroglucinol was strongly dependent on the initial amount of ZnO@TMSEDTA. It was found that surface modification of ZnO nanoparticles by silica resulted in fast interaction with the antibiotic. To our best knowledge it is the first time, that functionalized ZnO particles, synthesized at low temperature, coated by silica derivatives were obtained, and that their interactions with a drug were investigated by using electrochemistry measurements.

2 MATERIALS AND METHODS

2.1 Materials

The synthesis of ZnO was performed by using zinc acetate $Zn(CH_3COO)_2(H_2O)_2$ (Sigma–Aldrich) and ammonia, while the functionalization of ZnO was performed by using acetic acid glacial (CH_3COOH) from Baker Analyzed ACS Reagent (France) and N-(trimethoxysilylpropyl)ethylenediamine triacetic acid trisodium salt 45% in water from Gelest Inc. (PA, USA) and absolute ethanol from commercial alcohols (ON, Canada).

2.2 Preparation of ZnO

Aqueous ammonia (0.2 M) was slowly dripped at a rate of 30 mL h-1 in a solution of 100 mL of zinc acetate (0.1 M) to pH of 10. This mixture was kept at 60 °C for 12 h and then centrifuged for 20 min at a speed of 3800 rpm/min. Finally, the solid was rinsed several times with ultrapure water and ethanol by centrifugation and then dried in an oven for 1 h.

2.3 Functionalization reaction

Dispersion of 1.3 mg of ZnO was performed in an ultrasonic bath in 1 mL of absolute ethanol for 1 h. Thereafter, the dispersed ZnO nanoparticles were functionalized by the TMSEDTA under stirring for 4 h after addition of 10 μL of glacial acetic acid and 50 μL of the silane. The ZnO coating by TMSEDTA is rinsed successively with absolute ethanol, acetone and water to remove the free silane.

2.4 Electrochemical studies

The experiments were carried out using a potentiostat type Voltalab 40 (PGZ 301) and were conducted in 25 mL of 0.1 M phosphate buffer (pH 7.4) at 25 °C and the acquisition rate was set at 100 mV s^{-1}. A three-electrode configuration was used. The working electrode was a glassy carbon electrode (diameter 3 mm). The reference electrode was a saturated calomel electrode (SCE) and the counter electrode was a platinum wire. Cyclic voltammograms were done at different concentration of Phloroglucinol: 2.2 mM, 1.6 mM, 1.3 mM and 0.975 mM. Based on the intensity of the cathodic peak, a calibration curve was plotted, and a linear regression was obtained. This calibration curve was further used to deduce the drug uptake in the presence of ZnO@TSMEDTA nanoparticles. The voltage is scanned only from 0 to 1.2 V. The study focused on the oxidation part because the Phloroglucinol is not reducible. Experiments were done by following the signal decrease of the drug cathodic peak. Therefore, 6.3 mM of Phloroglucinol was put in solution. Then, 5 mg of functionalized particles was added, and the cyclic voltammetry measurement was performed. Five, 10 and 20 mg of particles were successively added to the previous solution and the voltammetric measurements were made again. These measurements allowed determining the drug uptake, which

is the total amount of drug loaded on the nanoparticles, and the drug uptake yield, which is the amount of attached drug as a function of the initial drug concentration. The results were the average of three experimental measurements.

2.5 Analysis equipment

2.5.1 X-ray diffraction

ZnO samples obtained were characterized by X-ray diffraction (Philips X-ray diffractometer Model PW 1730/10), and X-ray diffraction spectra were recorded by a diffractometer with radiation Philips X'pert POR Cu Ka (k = 1.5406 Å). The emission current, the scanning speed and the acceleration voltage are respectively equal to 40 mA, 0.02 h/s and 40 kV. Data acquisition is performed by a control unit and diffraction processing spectra are performed using the software ‘‘X'pert High score" containing the database JCPDS cards.

2.5.2 TEM

The NPs were also visualized using a FEI Tecnai Spirit Biotwin (JEOL, model JEM-1230, USA) transmission electron microscope (TEM) operating at an accelerating voltage of 120 kV. Drops of the NPs suspensions were deposited on carbon-coated copper grids. Size-distributions were extracted from the TEM images and the mean diameters of particles were measured using the Image J software (version 1.46; Wayne Rasband, National Institutes of Health, USA).

2.5.3 DLS

The hydrodynamic diameter of aqueous suspensions of Zn uncoated and coated particles was measured by dynamic light scattering (DLS) with a Nano S Zetasizer system (Malvern Instruments, Worcestershire, UK) using a laser (He-Ne) wavelength of 633 nm and a scattering angle of 173°. The temperature measurement was fixed at 25 °C. The viscosity and the refractive index of water were set to 0.8872 cp and 1.33. For Zn NPs, the refractive index was set to 2.008. The hydrodynamic diameter was calculated from the average of three measurements.

2.5.4 XPS

The surface chemical compositions of initial and functionalized NPs, as well as the binding state of TMSEDTA on ZnO particles, were investigated by XPS (PHI 5600-ci spectrometer, Physical Electronics U.S.A., MN, USA). Samples of particles were deposited and dried on gold coated silicon substrates previously cleaned by TL1 solutions (TL1 solution, a mixture of nanopure water, 30% H_2O_2 and 25% ammonia (Fisher, IL, USA) (5:1:1), at 80 °C for 10 min). The wafers were thoroughly rinsed with nanopure water and anhydrous ethanol and quickly dried under medical air. Functionalized Zn NPs in suspension were deposited on these substrates and the initial Zn NPs were directly deposited under powder. Both products were analyzed by XPS using a standard aluminum X-ray source for survey spectra (0–1400 eV) while high-resolution (HRXPS) spectra of C1s, O1s, Si2p, Zn2p3 were obtained using a standard magnesium X-ray source (1253.6 eV). Charge neutralization was not applied for either analysis. The detection was performed at 45° with respect to the surface normal and the analyzed area was 0.5 mm^2. The spectrometer work function was adjusted to give 285.0 eV for the main C (1s) peak. Curve fittings for high-resolution peaks were determined by means of the least squares minimization procedure employing Gaussian–Lorentzian functions and a Shirley-type background

2.5.5 FTIR analyses

The grafting efficiency of TMSEDTA on ZnO particles was also assessed by FTIR analyses. The crude NPs powder was deposited on a Si crystal whereas for the grafted NPs in suspension, solution drops were dried on the crystal. The measurements were performed by using Attenuated Total Reflectance mode (ATR) in FTIR (Agilent Cary 660 FTIR, Agilent technologies, Australia), equipped with a deuterated L-alanine-doped triglycine sulfate (DLa-TGS) detector and a Ge-coated KBr beam splitter.

2.5.6 TGA

The percentage of grafted DMSEDTA was evaluated by measuring the mass loss with a thermogravimetric analyzer (TGA 851 (Mettler-Toledo). Samples of the dried powders were deposited in a dedicated ceramic bowl for TGA, and the analyses were performed under nitrogen flow at a heating rate of 10 °C/min from 25 to 700 °C. From the TGA mass loss x, it can be deduced the amount of ligand molecules surrounding each particle as described by De Palma et al., by using the following formula:

$$N = \frac{\omega N_A \rho \frac{4}{3}\pi R^3 \times 10^{-23}}{MM} \quad (1)$$

where N is the number of ligands on each particle, R is the mean radius of the particle deduced from TEM images (in nm), q the density of the nanoparticles (5.605 g/cm^3), NA is Avogadro's number, and MM is the molar mass of the ligand.

3 RESULTS AND DISCUSSION

3.1 Characterization of the synthesized ZnO nanoparticles

XRD results (Fig. 1) show that the prepared solid is actually zinc oxide [ICCD 79-0207]. As can be seen, the peaks seen at 2θ = 31.737, 34.379, 36.215 and 47.484 correspond to the (100), (002), (101) and (102) diffraction planes, respectively.

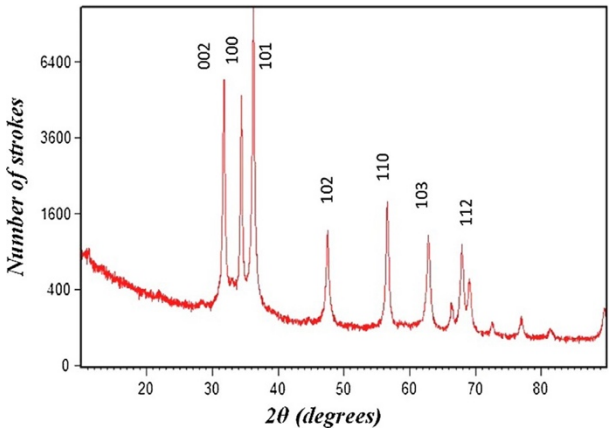

Figure 1. XDR pattern of ZnO NPs: X-axis: 2h (degrees); Y-axis: number of strokes.

The XRD results evidenced that the particles obtained were nanocrystalline and had a hexagonal Wurtzite structure. Moreover, it appears that the ZnO NPs had preferential a-axis and c-axis orientation along the (100) and (101) planes. In addition, the ZnO nanoparticles obtained exhibited

similar morphologies, as seen in TEM image (Fig. 2a) with nanometric sizes in which distribution ranged from 25 nm to 100 nm (Fig. 2b). The hydrodynamic size of the nanoparticles was then assessed by DLS measurements, leading to NPs hydrodynamic radius of 105 nm (average value – Fig. 2c). This value is quite in accordance with the results obtained from TEM and ImageJ software.

The characterization of the as-obtained ZnO particles confirms that it is possible to obtain nanocrystalline and quite well-distributed nanoparticles at low temperature (T = 60 °C). Moreover, the synthesis was done in ultrapure water as non-organic and non-toxic solvent in the absence of surfactants (Rao and Geckeler, 2011). Therefore, this new protocol hugely reduces the manufacturing cost of this material.

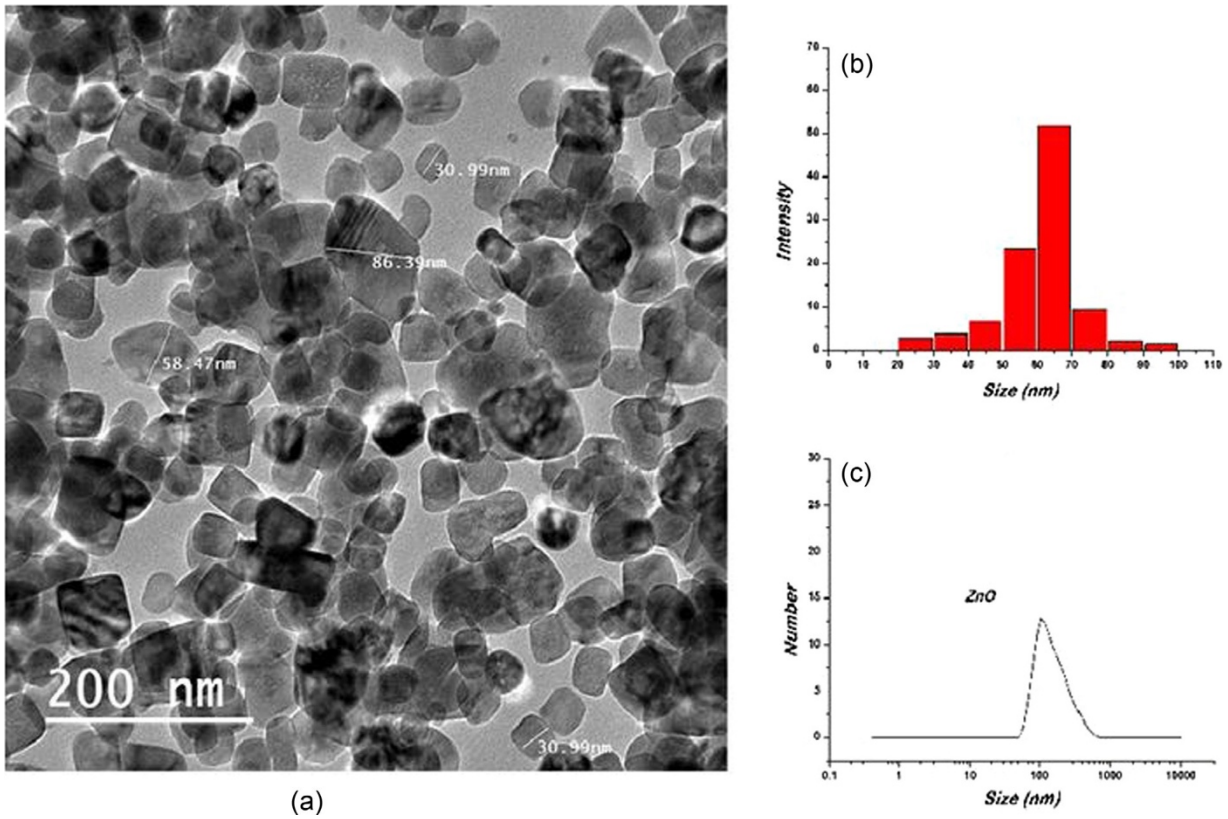

Figure 2. (a) TEM image of NPs ZnO; (b) size distribution from TEM analysis evaluated by ImageJ; (c) distribution of size by DLS analysis.

3.2 Functionalization of the ZnO nanoparticles

Silanization process was done in order to introduce chemical function on the as-synthesized particles to further graft the bioactive molecule. The functionalization with silane should be done in non-aqueous solution in order to avoid silane polymerization. It should also be processed in a solvent permitting a good dispersion of the nanoparticles, and a one enabling the hydrolysis of silane (-$Si(OMe)_3$ part) thus improving the efficacy of ZnO surface silanization. Therefore, the reaction has been done in absolute ethanol. The functionalization efficiency was assessed by surface characterization spectroscopy such as XPS and FTIR but also with TGA in order to determine the TMSEDTA's amount grafted on the ZnO nanoparticles surface.

Successful surface functionalization was confirmed by XPS analyses as seen in Table 1. Indeed, atomic surface compositions of the ZnO particles before and after functionalization were clearly different: increase in carbon from 7.0% to 45.8% with a decrease in Zn percentage due to the coating

presence, and detection of silicon as well as nitrogen coming from the TMSEDTA. These new atoms are associated with TMSEDTA molecules (Fig. 3). Moreover, as the C/Si ratios of theoretical and experimental after grafting, 11 and 12.05 respectively, are close it could be assumed that the hydrolysis of -Si(OMe)$_3$ was complete and led to optimize the coating, as mentioned by de Palma et al.

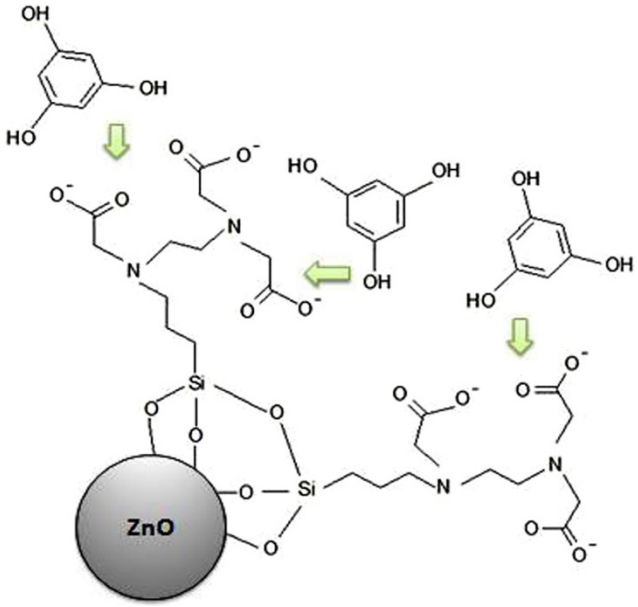

Figure 3. TMSEDTA molecules grafting on ZnO NPs and their interactions with Phloroglucinol.

It should also be noticed that the O/Zn ratio is close to 1 for the as-synthesized nanoparticles as expected, whereas after silanization step it is increased to 2.35. However, all the oxygen detected is not coming from the oxide (O-Metal bound) but also from the O associated with the coating (Fig. 4). Considering the band at 530.0 eV associated with Zn-O in which contribution is 12.7% and that the relative percentage of Zn is 12.8%, the O/Zn ratio remained 1, meaning that the ZnO structure was kept and was not affected by the reaction medium (no hydroxylation as well as degradation). Furthermore, only one peak centered on 1021 eV for Zn2p high resolution spectrum was detected, whose binding energy is mainly associated with Zn^{2+} form linked to O.

Table 1 Surface atomic composition of ZnO nanoparticles before and after functionalization with TMSEDTA.

	C1s	O1s	Zn2p3	N1s	Si2s	Na1s
As-synthesized	7.0	47.1	45.9	0	0	0
ZnO@TMSEDTA	45.8	30.1	12.8	5.0	3.8	2.5

The two other peaks in XPS HR spectra of O1s were centered at 532.0 and 534.0 eV and are associated with the oxygen of TMSEDTA, O=C/C-O/Zn-O-Si and Si-O (De Palma et al., 2007) bonds, respectively (Jayalakshmi et al., 2013). The region of C1s exhibits 4 peaks centered at 285.0, 286.5, 289.0 and 291.4 eV assigned to C-C/C-H bonds, C-O/C-N, C(O)OH and C(O)O^-, respectively

(Bhunia et al., 2012). It is interesting to notice that there are carboxylate and carboxylic acid groups (3.9% and 6.0%), which could be then involved in the interaction with Phloroglucinol. Regarding the chemical structure of TMSEDTA when grafted (Fig. 3), it should be expected 1 Si for 3 carbonyl and the ratio observed is 1 for 2.6 (3.8% of Si on 9.9% of carbonyl). This result confirms once again that the silanization reaction occurred as expected and that the functionalization was fully successful.

The grafting efficiency of TMSEDTA on ZnO was also confirmed by FTIR analyses which clearly exhibited the expected bands as seen in Fig. 5. Indeed, the intense peaks located at 1602 cm^{-1} and 1393 cm^{-1} were assigned to the asymmetric and symmetric stretching mode vibration of COO^- groups (carboxylic acid) (Carpio et al., 2014). Features centered at 2928 cm^{-1} are due to stretching mode of methylene groups (De Palma et al., 2007) while the O-H stretching mode vibration band is centered at 3370 cm^{-1} (Carpio et al., 2014). The tertiary amine C-N is also evidenced by its stretching vibration centered at 1204 cm^{-1}. The band at 1017 cm^{-1} resulting from Si-O-Si stretching vibrations permits to confirm the silanization with the surface of ZnO nanoparticles (Aizawa and Shaffer, 2003). Moreover, outgoing bands at 1095 cm^{-1} and 917 cm^{-1} indicate the formation of Si-O-Zn bonds (Dupont et al., 2014). These results corroborated the XPS results and also the efficiency of the silanization reaction. It should also be noticed that in XPS both carboxylate and carboxylic acid were observed whereas in FTIR, mainly carboxylates were detected with a slight shoulder at 1725 cm^{-1} associated with COOH group. This observation could be explained by the fact that the asymmetric vibration of COO^- is very large and covered the carboxylic acid one which was further shifted due to H bonds (Coates, 2000).

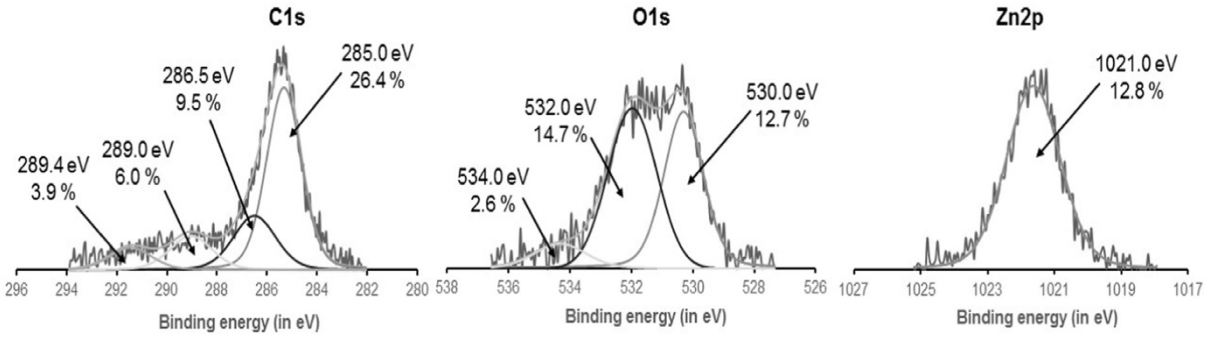

Figure 4. XPS high resolution spectra of C1s, O1s and Zn2p of TMSEDTA@ZnO.

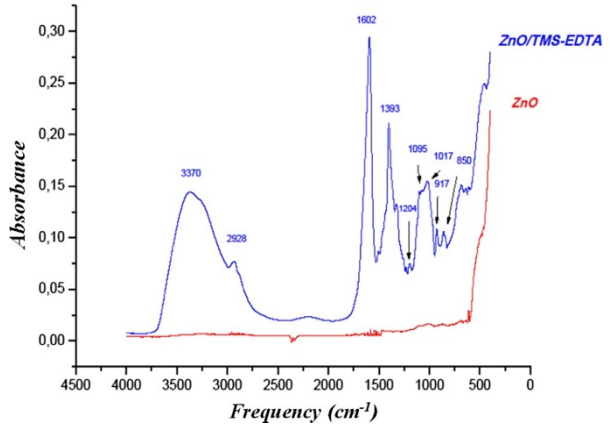

Figure 5. FTIR spectra of ZnO and ZnO@TMSEDTA.

All these spectroscopy techniques have clearly evidenced the grafting efficiency of TMSEDTA on ZnO nanoparticles. In order to quantify the NPs covering, TGA measurements were then done.

Indeed, based on the weight loss, 10.2% in this case, the amount of TMSEDTA molecules grafted per ZnO nanoparticle was therefore estimated (details described in experimental part) and led to 11.85 x 10^6 molecules of TMSEDTA per nanoparticle. Compared to de Palma et al., 2495 molecules per NPs for the same ligand, this covering appears quite high. However, their NPs got a radius of 4.3 nm whereas our ZnO NPs are more 32.5 nm, meaning that in volume the NPs are 1000 more than their ones. Furthermore, in their case, they mentioned that they had a high amount silane layer due to the formation of a polymerized silane multilayer which limits the covering of the nanoparticles itself. Therefore, based on this, it could be assumed that ZnO@TMSEDTA NPs exhibited a good covering made of a dense silane monolayer. To our knowledge, this is the first time that ethanol was used for dispersion of NPS ZnO and as solvent for the silanization reaction. The non-toxic property of ethanol, compared to other organic solvents, and the stability of dispersed ZnO NPs are two advantages of this method of silane grafting.

3.3 Loading of the functionalized ZnO nanoparticles with the bioactive molecule

The functionalized NPs, ZnO@TMSEDTA, were further used in order to assess their ability to interact with Phloroglucinol, which is a drug used in antispasmodic treatment, and, which has been also included in pesticides and cement (Singh et al., 2010). First, cyclic voltammograms of various drug concentrations in phosphate buffer, 0.975, 1.3, 1.6 and 2.2 mM have been performed.

Fig. 6 shows the cyclic voltammograms obtained after the drug addition. These cyclic voltammograms have been used to trace the calibration curve of the current intensity according to the various concentrations of the Phloroglucinol (the inset). As seen in Fig. 6, the characteristic peak of the drug located at 0.62 V underwent an increase when Phloroglucinol was added in the solution. The inset evidences an excellent correlation between the current intensity and the drug concentration (R^2 = 0.993), meaning that this technique is accurate to quantify the drug.

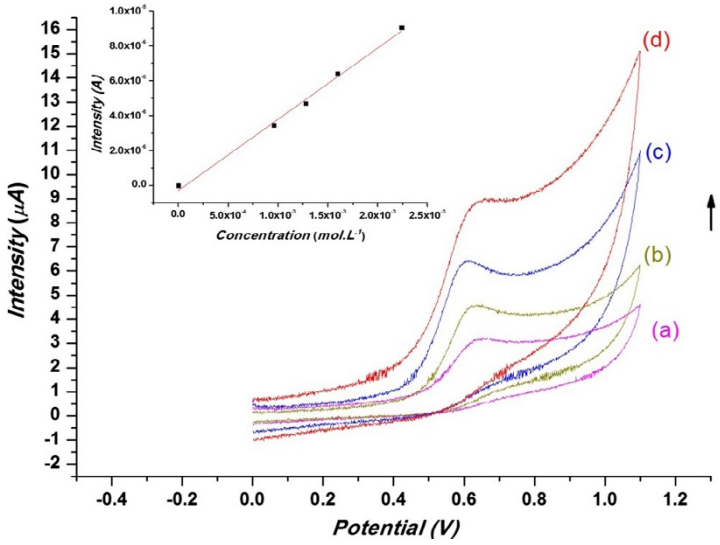

Figure 6. Cyclic voltammograms for a different concentration of the Phloroglucinol. Calibration graph of the current intensity v Phloroglucinol concentration in 25 mL phosphate buffer (a 0.975 mM of the Phloroglucinol, (b) 1.3 mM of the Phloroglucinol (c) 1.6 mM of the Phloroglucinol, (d) 2.2 mM of the Phloroglucinol.

Thereafter, voltammetry measurements were done by adding step by step the functionalized ZnO particles, from 5 mg/ mL to 40 mg/mL, to the drug solution (Fig. 7). Compared with the cyclic voltammogram of (a), the current intensity of the drug was unaffected despite adding a vast amount

of the uncoated ZnO NPs (b). This observation means that no interaction occurred between the uncoated NPs and the drug. It should also be noticed that there was a slight shift in the potential value (from 0.62 V to 0.66 V). However, the addition of functionalized particles, ZnO@TMSEDTA led to a decrease in the current density (Fig. 7 c–f), which proved that there are interactions between the ZnO@TMSEDTA and the Phloroglucinol.

Based on the calibration curve equation, obtained from Fig. 6, I = 0.00507 x C, where I is the current intensity (A) and C is the drug concentration (M), the drug concentration uptake on ZnO@TMSEDTA NPs could be therefore deduced. In this case, the intensity value considered is the difference, DI, between the intensity of free Phloroglucinol from curve (a) with the one of other curve (Fig. 7c–f respectively). The results are summarized in Table 2.

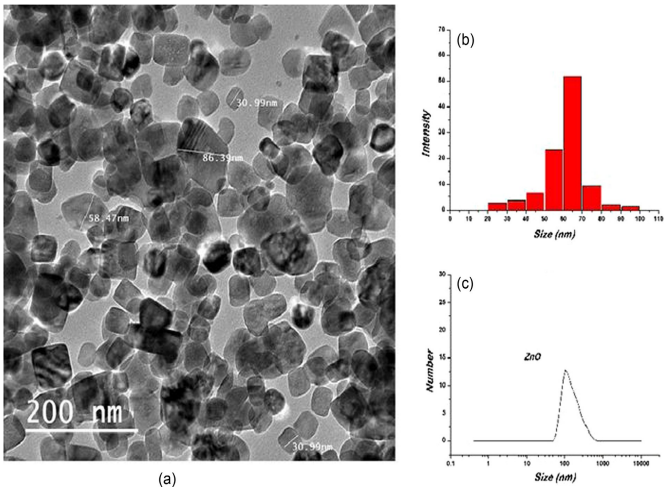

Figure 7. (a) The cyclic voltammograms analysis for Phloroglucino (6.3 mM), (b) Phloroglucinol (6.3 mM) with 80 mg of ZnO (c) Phloroglucinol (6.3 mM) with ZnO@TMS.EDTA (5 mg), (d) Phloroglucinol (6.3 mM) with ZnO@TMS.EDTA (10 mg), (e) Phloroglucinol (6.3 mM) with ZnO@TMS.EDTA (20 mg), (f) Phloroglucinol (6.3 mM) with ZnO@TMS.EDTA (40 mg).

The drug concentration uptake was clearly evidenced with functionalized NPs (c–f) compared to uncoated ones (b), and the decrease in intensity appeared to be dependent on the amount of coated particles introduced in the medium. Indeed, as it could be expected more NPs in suspension led to higher amount of drug uptake, thus leading to a better uptake yield (ratio between the drug concentration uptake with the initial drug amount in solution). However, increasing ZnO@TMSEDTA concentrations led to lower decrease in intensities (Fig. 7d–f) compared to the first uptake (Fig. 7c). It could be explained by the fact that already 40% of initial Phloroglucinol was capped by the 5 mg/mL of NPs, thus leading to less free drug in solution for the particles added thereafter.

Regarding the interactions between the functionalized ZnO particles and the Phloroglucinol, they could be due to electrostatic interactions or to hydrogen bounds between the phenolic OH of the drug and the carboxylic acid functions of the TMSEDTA. These links are of low energies and appeared reversible. Indeed, after agitation, the new cyclic voltammogram exhibited the same current intensity of free Phloroglucinol in solution at 6.3 mM, without ZnO@TMSEDTA particles. Therefore, all the drug molecules trapped in ZnO@TMSEDTA could be easily removed from the solution. This result is very important because the drug can be easily quantified in polluted water, removed from the ZnO@TMSEDTA particles which ones could be regenerated and reused after analysis. As already mentioned, the speed detection and the ease of separation between a drug and the ZnO@TMSEDTA are specific criteria. These requirements are important for the manufacturing of the electrochemistry cell in drug development detection.

Table 2 Evaluation of the drug uptake and drug uptake efficiency on ZnO NPs.

Curve	Mass (mg)	ΔI (μA)	Drug uptake (mM)	Uptake yield (%)
(a) Free drug	–	0	0	0
(b) ZnO	80	0.41	0.08	1.26
(c) ZnO@TMEDTA	5	12.77	2.55	40.47
(d) ZnO@TMEDTA	10	15.52	3.10	49.20
(e) ZnO@TMEDTA	20	16.81	3.36	53.33
(f) ZnO@TMEDTA	40	19.30	3.86	60.79

4 CONCLUSION

The synthesis of the ZnO nanoparticles was performed with an original protocol in surfactant-free aqueous solutions at relatively low temperature, therefore allowing to produce ZnO nanoparticles at low cost. The resulting ZnO particles exhibited the expected crystallinity structure, as evidenced by XRD result, and relatively well distributed sizes ranging from 25 to 100 nm, as seen by TEM analyses. The silanization of the crude ZnO particles was verified by spectroscopy techniques, such as FTIR and XPS. Both characterizations evidenced the efficiency of the functionalization step. Also, the TGA measurement proved the efficacy of silanization with a loss of 10.2%, meaning that there was a high amount of silane molecules per particles. Compared to literature, it could also be assumed that TMSEDTA@ZnO NPs exhibited a good covering made of a dense silane monolayer. This coating exhibited carboxylic groups that can further interact with the phenolic groups of the investigated drug, the Phloroglucinol. The drug-material interactions were thus assessed by electrochemical method. The cyclic voltammograms showed significant interactions in spite of low concentrations of the drug, and exhibited a fast degradation of Phloroglucinol cathodic peak, in less than 2 min. These results proved the high sensibility of ZnO@TMSEDTA toward the Phloroglucinol, and the material could be used as Phloroglucinol sensor in polluted solution. Besides, these interactions are reversible; thus, the particles could be further reused. In the event, this material proved to be a practical way of determining the presence of drug in water solution. Further investigations will be done in more complex solutions such as ‘‘real” polluted water and milk, but also regarding an electrode made of ZnO@TMSEDTA or doped with these particles.

ACKNOWLEDGEMENTS

The authors gratefully acknowledge the professional research Andrée-Anne Guay-Bégin and Stéphane Turgeon from Laboratoire d’Ingénierie de Surface (LIS) for the help.

REFERENCES

Acuautla, M., Bernardini, S., Gallais, L., Fiorido, T., Patout, L., Bendahan, M., 2014. Ozone flexible sensors fabricated by photolithography and laser ablation processes based on ZnO nanoparticles. Sens. Actuat. B – Chem. 203, 602.
Aizawa, M., Shaffer, M.S.P., 2003. Silylation of multi-walled carbon nanotubes. Chem. Phys. Lett. 368, 121.
Chan, K.L. Andrew, Fale, P.L.V., 2014. Label-free in situ quantification of drug in living cells at micromolar levels using infrared spectroscopy. Anal. Chem. 86, 11673.
Bailly, E., Levi, Y., Karolak, S., 2013. Calibration and field evaluation of polar organic chemical integrative sampler (POCIS) for monitoring pharmaceuticals in hospital wastewater. Environ. Pollut. 174, 100.
Bhunia, P., Hwang, E., Min, M., Lee, J., Seo, S., Some, S., Lee, H., 2012. A non-volatile memory device consisting of graphene oxide covalently functionalized with ionic liquid. Chem. Commun. 48, 913.

Cao, B., Xu, H., Mao, C., 2011. Controlled self-assembly of rodlike bacterial pili particles into ordered lattices. Angew. Chem. Int. Ed. 50, 6264.
Carpio, I.E.M., Mangadlao, J.D., Nguyen, H.N., Advincula, R.C., Rodrigues, D.F., 2014. Graphene oxide functionalized with ethylenediamine triacetic acid for heavy metal adsorption and anti-microbial applications. Carbon 77, 289.
Choi, S., Kim, S.S., 2012. Room temperature CO sensing of selectively grown networked ZnO nanowires by Pd nanodot functionalization. Sens. Actuat. B – Chem. 168, 8.
Coates, John, 2000. Interpretation of Infrared Spectra. A Practical Approach Encyclopedia of Analytical Chemistry. John Wiley & Sons Ltd., Chichester, p. 10815.
De Palma, R., Peeters, S., Van Bael, M.J., Van den Rul, H., Bonroy, K., Laureyn, W., Mullens, J., Borghs, G., Maes, G., 2007. Silane ligand exchange to make hydrophobic superparamagnetic nanoparticles water-dispersible. Chem. Mater. 19, 1821.
Deng, Z., Rui, Q., Yin, X., Liu, H., Tian, Y., 2008. In vivo detection of superoxide anion in bean sprout based on ZnO nanodisks with facilitated activity for direct electron transfer of superoxide dismutase. Anal. Chem. 80, 5839.
Dennison, M.J., Turner, A.P.F., 1995. Biosensors for environmental monitoring. Biotech. Adv. 13, 1.
Desmet, C., Blum, L.J., Marquette, C.A., 2012. High-throughput multiplexed competitive immunoassay for pollutants sensing in water. Anal. Chem. 84, 10267.
De´ vier, M.H., Le Menach, K., Viglino, L., Di Gioia, L., Lachassagne, P., Budzinski, H., 2013. Ultra-trace analysis of hormones, pharmaceutical substances, alkylphenols and phthalates in two French natural mineral waters. Sci. Total Environ. 443, 621.
Do¨ nmez, S., Arslan, F., Sarı, N., Yetim, N.K., Arslan, H., 2014. Preparation of carbon paste electrodes including poly(styrene) attached glycine–Pt(IV) for amperometric detection of glucose. Biosens. Bioelectron. 54, 146.
Duan, Y., Dai, C., Zhang, Y., Chen, L., 2013. Selective trace enrichment of acidic pharmaceuticals in real water and sediment samples based on solid-phase extraction using multi-templates molecularly imprinted polymers. Anal. Chim. Acta 758, 93.
Dupont, D., Brullot, W., Bloemen, M., Verbiest, T., Binnemans, K., 2014. Selective uptake of rare earths from aqueous solutions by EDTA-functionalized magnetic and nonmagnetic nanoparticles. ACS Appl. Mater. Interfaces 6, 4980.
Guan, H., Zhang, F., Yu, J., Chi, D., 2012. The novel acetylcholinesterase biosensors based on liposome bioreactors-chitosan nanocomposite film for detection of organophosphates pesticides. Food Res. Int. 49, 15.
Gupta, A., Kim, B.C., Edwards, E., Brantley, C., Ruffin, P., 2012. Covalent functionalization of zinc oxide nanowires for high sensitivity p-nitrophenol detection in biological systems. Mater. Sci. Eng. B 177, 1583.
Huang, Z., Yan, D., Yang, M., Liao, X., Kang, Y., Yin, G., Yao, Y., Hao, B., 2008. Preparation and characterization of the biomineralized zinc oxide particles in spider silk peptides. J. Colloid Interface Sci. 325, 356.
Irajizad, A., Mortezaali, A., 2015. Room temperature H2S gas sensor based on rather aligned ZnO nanorods with flower-like structures. Sens. Actuat. B – Chem. 207, 865.
Jayalakshmi, G., Gopalakrishnan, N., Balasubramanian, T., 2013. Activation of room temperature ferromagnetism in ZnO films by surface functionalization with thiol and amine. J. Alloys Compd. 551, 667.
Li, X., He, G., Han, Y., Xue, Q., Wu, X., Yang, S., 2012. Magnetic titania-silica composite-polypyrrole core–shell spheres and their high sensitivity toward hydrogen peroxide as electrochemical sensor. J. Colloid Interface Sci. 387, 39.
Li, X., Yao, J., Liu, F., He, H., Zhou, M., Mao, N., Xiaoa, P., Zhang, Y., 2013. Nickel/copper nanoparticles modified TiO2 nanotubes for nonenzymatic glucose biosensors. Sens. Actuat. B – Chem. 181, 501.

Marcu, A., Viespe, C., 2015. Laser-grown ZnO nanowires for roomtemperature SAW-sensor applications. Sens. Actuat. B – Chem. 208, 1.
Mora, M.F., Giacomelli, C.E., Garcia, C.D., 2007. Electrophoretic effects of the adsorption of anionic surfactants to poly(dimethylsiloxane)-coated capillariesn. Anal. Chem. 79, 6675.
Qian, J., Yang, X., Jiang, L., Zhu, C., Mao, H., Wang, K., 2014. Facile preparation of Fe3O4 nanospheres/reduced graphene oxide nanocomposites with high peroxidase-like activity for sensitive and selective colorimetric detection of acetylcholine. Sens. Actuat. B – Chem. 201, 160.
Rao, J.P., Geckeler, K.E., 2011. Polymer nanoparticles: preparation techniques and size-control parameters. Progr. Polym. Sci. 36, 887. Shukla, S.K., Deshpande, S.R., Shukla, S.K., Tiwari, A., 2012. Fabrication of a tunable glucose biosensor based on zinc oxide/chitosan-graft-poly(vinyl alcohol) core–shell nanocomposite. Talanta 99, 283.
Singh, I.P., Sidana, J., Bharate, S.B., Foley, W.J., 2010. Phloroglucinol compounds of natural origin: synthetic aspects. Nat. Prod. Rep. 27, 393.
Su, Q., Ma, X., Dong, J., Jiang, C., Qian, W., 2011. A reproducible SERS substrate based on electrostatically assisted APTES-functionalized surface-assembly of gold nanostars. ACS Appl. Mater. Interfaces 3, 1873.
Tan, G., Zhang, L., Ning, C., Liu, X., Liao, J., 2011. Preparation and characterization of APTES films on modification titanium by SAMs. Thin Solid Films 519, 4997.
Wang, F., Li, D., Mao, C., 2008. Genetically modifiable flagella as templates for silica fibers: from hybrid nanotubes to 1D periodic nanohole arrays. Adv. Funct. Mater. 18, 4007.
Wang, F., Nimmo, L.S., Caoa, B., Mao, C., 2012. Oxide formation on biological nanostructures via a structure-directing agent: towards an understanding of precise structural transcription. Chem. Sci. 3, 2639. Wang, Y., Ju, Z., Cao, B., Gao, X., Zhu, Y., Qiu, P., Xu, H., Pan, P.,
Bao, H., Wang, L., Mao, C., 2015. Ultrasensitive rapid detection of human serum antibody biomarkers by biomarker-capturing viral nanofibers. ACS Nano 9, 4475.
Xie, Y., Hill, C.A.S., Xiao, Z., Militz, H., Mai, C., 2010. Silane coupling agents used for natural fiber/polymer composites: a review. Compos. Part A – Appl. Sci. 41, 806.
Yu, P., Chang, C., Chiu, C., Yang, C., Yu, Ju., Kuo, H., Hsu, S., Chang, Y., 2009. Efficiency enhancement of GaAs photovoltaics employing antireflective indium tin oxide nanocolumns. Adv. Mater. 21, 1001.
Zaideh, B.I., Saad, N.M.R., Lewis, B.A., Brenna, J.T., 2001. Reduction of nonpolar amino acids to amino alcohols to enhance volatility for high-precision isotopic analysis. Anal. Chem. 73, 799.